Thermal Hydraulics Analysis for Cooling Tower Performance

Si Y. Lee and Alfred J. Garrett
Savannah River National Laboratory
si.lee@srnl.doe.gov and alfred.garrett@srnl.doe.gov

Abstract

Mechanical Draft Cooling Towers (MDCT's) are used in industrial processes to dissipate waste heat by transferring heat from water to air via evaporative cooling, which causes air humidification. The Savannah River Site (SRS) has two different types of the cooling towers, cross-flow cooling tower located in A-Area and the other is counter-current cooling tower located in H-Area. MDCT typically consists of four independent compartments called cells. Each cell has its own fan to help maximize heat transfer between ambient air and circulated water. The primary objective of the work is to conduct a parametric study for cooling tower performance under different fan speeds and ambient air conditions.

The Savannah River National Laboratory (SRNL) developed a Computational Fluid Dynamics (CFD) model to achieve the objective. The model uses three-dimensional momentum, energy, continuity equations, air-vapor species balance equation, and two-equation turbulence as the basic governing equations. It was assumed that vapor phase is always transported by the continuous air phase with no slip velocity. In this case, water droplet component was considered as discrete phase for the interfacial heat and mass transfer via Lagrangian approach. Thus, the air-vapor mixture model with discrete water droplet phase is used for the analysis.

A series of the modeling calculations was performed to investigate the impact of ambient and operating conditions on the thermal hydraulic performance of the cooling tower when fans were operating and when they were turned off. The model was benchmarked against the literature data and the SRS test results for key parameters such as air temperature and humidity at the tower exit and water temperature for given ambient conditions. The test and modeling results for the two types of SRS cooling towers are discussed here, focusing on the performance analysis of the countercurrent cooling tower in H-Area, since the modeling analysis of the cross-flow cooling tower in A-Area was presented in the previous paper.

KEYWORDS
Cooling Tower, Computational Fluid Dynamics, Heat Transfer, Mechanical Draft Cooling Tower

1. INTRODUCTION

Mechanical Draft Cooling Towers (MDCT) are designed to cool process water via sensible and latent heat transfer to air. Heat and mass transfer take place simultaneously. Heat is transferred as sensible heat due to the temperature difference between liquid and gas phases, and as the latent heat of the water as it evaporates. Mass of water vapor is transferred due to the difference between the vapor pressure at the air-liquid interface and the partial pressure of water vapor in the bulk of the air.

The primary objective of the work is to conduct a parametric study for cooling tower performance under different fan speeds and ambient air conditions. Another purpose of the work is to develop a model to evaluate the flow patterns inside the cooling tower cell driven by cooling fan and wind, considering the cooling fans to be on or off. The Savannah River National Laboratory (SRNL) made experimental measurements and observations and developed a Computational Fluid Dynamics (CFD) model to achieve the objective [1]. Savannah River Site (SRS) has two types of the cooling towers to be studied here. One is a cross-flow cooling tower located in A-Area, and the other is a countercurrent cooling tower located in

H-Area. The cooling tower located in A-Area consists of four compartment cells. It is 13.7m wide, 36.8m long, and 9.4m high. Each cell has its own cooling fan and shroud without any flow communications between two adjacent cells. There are water distribution decks on both sides of the fan shroud. The deck floor has an array of about 25mm size holes through which water droplet falls into the cell region cooled by the ambient air driven by fan and wind, and it is eventually collected in basin area. Detailed descriptions and modeling results for the cross-flow MDCT are provided in the previous paper [2]. The H-Area cooling tower is about 7.3 m wide, 29.3 m long, and 9.0 m high as illustrated in Fig. 1. Each cell has its own cooling fan and shroud, but each of two corner cells has two panels to shield wind at the bottom of the cells. There is some degree of flow communications between adjacent cells through the 9-in gap at the bottom of the tower cells as shown in Fig. 1. Detailed geometrical dimensions for the H-Area MDCT configurations are presented in the figure.

The model was benchmarked and verified against the literature and SRNL test results. The verified model was applied to the investigation of cooling fan and wind effects on water cooling in cells when fans are off and on. The previous paper [2] presented the validation results for key physical models with the literature results and the integral benchmarking results against the test results for the cross-flow MDCT system in A-Area. This paper will mainly discuss the results for the countercurrent flow MDCT in H-Area and compare the results for the two different types of MDCT's.

2. MODELING APPROACH AND SOLUTION METHOD

The present work took a three-dimensional CFD approach. The modeling domain was parallelepiped, and it was about 8 times larger than the actual size of the four-cell MDCT in Fig. 1 to calculate the air flow patterns inside and outside the tower cells. Cooling fan of each cell was modeled as momentum source at the shroud region since air velocity at shroud exit was continuously measured. The air-vapor mixture model was considered, assuming that vapor phase is always transported by the continuous air phase with no slip. In this situation, water droplet component was considered as discrete phase for the interfacial heat and mass transfer to air via Lagrangian approach. The force balance for each droplet equates the particle inertia with forces acting on a spherical particle of uniform size, d_p. In this work, water distributions at the inlet of the water droplet are assumed to be uniform for computational efficiency although about 20% of non-uniform distributions are shown by the initial test results. Thus, the air-vapor mixture model coupled with discrete water droplet phase is used for the analysis.

The governing equations to be solved for the modeling domain are one air-vapor mixture balance, one vapor species transport, three momentum conservations along x-, y-, and z- coordinate systems for the modeling domain, two standard turbulence equations, and one air-vapor mixture energy balance. κ–ε standard turbulent model is used for simulation of the turbulent airflow. All governing equations and constitutive relations to be solved for the computational domain are shown in Eqs. (1) to (24). Droplet momentum balance and heat and mass transfer balance equations, Eq. (6) to (16), are solved by Lagrangian integral approach along the particle trajectory from water droplet inlet to the exit. The modeling constants and gas properties are updated by the constitutive relations as provided by Eqs. (17) to (24). All governing equations and constitutive relations used for the calculations are discussed below in a brief way.
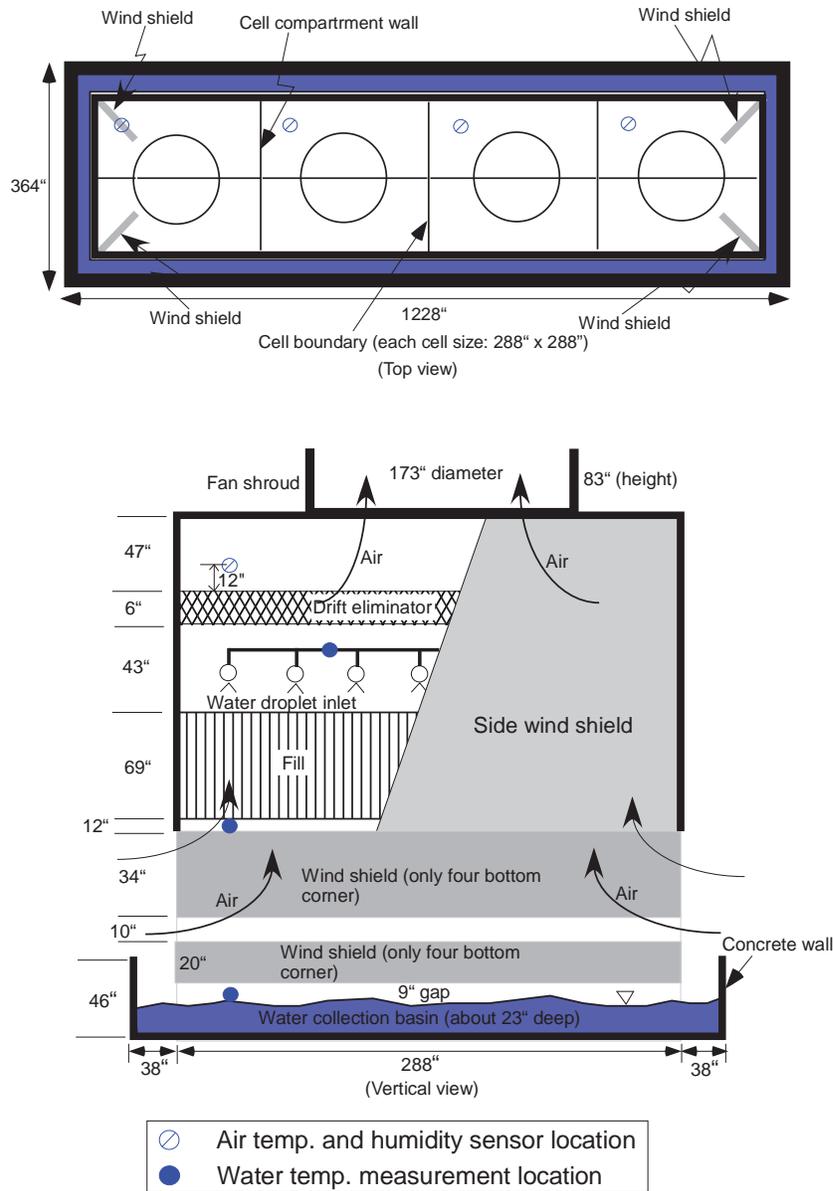
Figure 1. Top-down view and cross-section view of the compartment cell instrumented for the performance measurement for H-area cooling tower (1" = 0.0254 m).

Mass conservation equation:

$$\nabla \bullet \left(\rho \bar{v} \right) = S_v \tag{1}$$

where ρ and v are fluid density and velocity. S_v in the equation is a source term of vapor species added to the air due to the evaporation of the dispersed water droplets.

Momentum conservation equation:

$$\nabla \bullet (\rho \bar{v}\bar{v}) = -\nabla p + \nabla \bullet (\bar{\tau}) + \rho \bar{g} + \bar{F} \tag{2}$$

In Eq. (2) $\bar{\tau}$ is shear stress, and g is acceleration due to gravity. $\bar{F}$ is external force from interaction with the dispersed phase.

Energy conservation equation:

$$\nabla \bullet \{\bar{v}(\rho h_{sm} + 0.5\rho v^2)\} = \nabla \bullet (k_{h,eff}\nabla T - h_{sv}\bar{J}_v) \tag{3}$$

where h_{sm} is sensible specific enthalpy of the gas mixture, and $k_{h,eff}$ is effective thermal conductivity. h_{sv} and J_v are sensible specific enthalpy and diffusion flux of vapor species, respectively. T is the mixture temperature.

Turbulence equations based on two-equation model:

The present analysis used a two-equation model, referred to as k-ε model in the literature [3]. In this model, transport equations are solved for two turbulence quantities, turbulence kinetic energy (k) and turbulence energy dissipation rate (ε) to capture the turbulent energy dissipation process of air humidification through each of the four MDCT cells. Empirical balance equations for these two modeling parameters are provided in the literature [1,3].

Species Transport Equation:

Conservation equation for vapor species is governed by

$$\nabla \cdot (\rho \bar{v}Y_v) = -\nabla \cdot \bar{J}_v + S_v \tag{4}$$

Y_v is local mass fraction of vapor in the continuous air. $\bar{J}_v$ is diffusion flux of vapor species. The diffusion flux of water vapor under turbulent air flow is computed by

$$\bar{J}_v = -\left(\rho D_v + \frac{\mu_t}{Sc_t}\right)\nabla Y_v \tag{5}$$

D_v is molecular diffusion coefficient of water vapor in the continuous air medium. Sc_t is turbulent Schmidt number.

Momentum Balance for Discrete Water Droplet

Force balance for droplet is considered along the particle trajectory in a Lagrangian reference frame. The force balance equates the particle inertia with forces acting on a spherical particle of uniform size, d_p.

$$\frac{d}{dt}u_p = F_{Di} + F_g + F_{vm,x} + F_{pg,x}$$
$$= \frac{3}{4}C_D\left(\frac{\mu Re}{\rho_p d_p^2}\right)(u - u_p) + \left(\frac{\rho_p - \rho}{\rho_p}\right)g_x + F_{vm,x} + F_{pg,x} \tag{6}$$

In the above equation, Re and $F_{vm,x}$ are Reynolds number based on droplet diameter d_p and additional force due to virtual mass effect, respectively. Subscripts, D and p, of each parameter stands for drag and

water droplet, respectively. Coefficient C_D in the first term of the right-hand side is drag coefficient on the droplet surface due to the upward air motion. The drag coefficient for the spherical droplet particle as used by Morsi and Alexander (1972) was applied to the calculations. The last term $F_{pg,x}$ is lift force due to pressure gradient in the fluid side. That is,

$$\mathrm{Re} = \frac{\rho d_p |u - u_p|}{\mu} \tag{7}$$

$$F_{vm,x} = \frac{1}{2} \frac{\rho}{\rho_p} \frac{d}{dt}(u - u_p) \approx 0 \text{ since } \rho_p \text{ is much larger than the air density } \rho. \tag{8}$$

$$F_{pg,x} = \frac{\rho}{\rho_p} u_p \frac{\partial u}{\partial x} \tag{9}$$

Heat and Mass Balance for Discrete Droplet

The droplet temperature is updated along the particle trajectory according to a heat balance with no radiation cooling,

For $T_{vap} \leq T_p < T_{boiling}$

$$m_p C_p \frac{dT_p}{dt} = hA_p(T - T_p) + \frac{dm_p}{dt} h_{fg} \tag{10}$$

Heat transfer coefficient h in the above equation is calculated from a literature correlation [5].

$$Nu = \frac{hd_p}{k_{h,eff}} = 2.0 + 0.6\,\mathrm{Re}_d^{0.5}\,\mathrm{Pr}^{\frac{1}{3}} \tag{11}$$

Nusselt number, Nu, in Eq. (11) is defined as the ratio of local average convective transfer to conduction-controlled heat transfer, which is very similar to a mass-transfer Sherwood number, Sh, as will be discussed later. Heat transfer coefficient, h, for convective heat flux, the first term in the right-hand-side of Eq. (10), is calculated by the literature correlation Eq. (11). The parameter $k_{h,eff}$ is effective thermal conductivity. Reynolds number Re_d is based on the particle diameter d_p and the relative velocity as define by Eq. (7). Prandtl number Pr is defined as the ratio of viscous diffusion to conduction for the continuous air phase ($C_p\mu/k$).

Rate of evaporation $\dfrac{dm_p}{dt}$ in Eq. (10) is computed from the mass transfer equation. Mass transfer at the surface of water droplet is governed by the concentration gradient. The mass flux ϕ at the surface of each droplet is given by

$$\phi = k_m(C_{vp} - C_v) \tag{12}$$

In Eq. (12) k_m is mass transfer coefficient. In this case the mass concentration of vapor at the droplet surface, C_{vp}, is estimated by assuming that the partial pressure of vapor at the interface is equal to the saturated vapor pressure, p_{sat}, at the droplet temperature, T_p.

$$C_{vp} = \frac{p_{sat}(T_p)}{RT_p} , \text{ where } R \text{ is universal gas constant.} \tag{13}$$

The concentration of vapor in the bulk gas, C_v, is known from solution of the transport equation for vapor species when local mole fraction of vapor species is given by X_v at local pressure p and temperature T.

$$C_v = M_{H2O} X_v \frac{p}{RT} \tag{14}$$

where M_{H2O} = molecular weight of vapor

Mass transfer coefficient k_m in the above equation is calculated from a literature correlation by using a similarity between heat transfer and mass transfer [5,6].

$$Sh = \frac{k_m d_p}{D_v} = 2.0 + 0.6 \, Re_d^{0.5} \, Sc^{\frac{1}{3}} \tag{15}$$

where Sherwood number, Sh, is defined as the ratio of local average mass transfer to diffusion-controlled mass transfer, which is sometimes called a mass-transfer Nusselt number, Nu. Nondimensional number Sc in the eaquation is defined as the ratio of viscous to mass diffusions, $\mu/\rho D_v$, where D_v is diffusion coefficient of vapor in the bulk. Using the mass transfer coefficient, k_m, calculated by Eq. (15), vapor mass flux ϕ_m is computed by Eq. (12). The vapor mass flux becomes a source term of vapor species S_v in the vapor species transport equation Eq. (4).

As result of the evaporation of water droplet, the mass of the droplet is reduced after time interval dt according to

$$\frac{dm_p}{dt} = -\phi_m A_p \tag{16}$$

where m_p = mass of the droplet
A_p = surface area of the water droplet

Change rate of droplet mass due to the evaporation process is coupled with the droplet heat balance equation Eq. (10), resulting in updating the overall energy balance equation for the mixture.

Constitutative Relations

- q''' (Amount of sensible heat transfer from water to air inside the cell compartment excluding the latent of heat under different ambient humidity and operating conditions)
- ρ (Density relations to account for humidity)

Dry air density, ρ_a, is calculated from the equation of state for ideal gas. That is

$$\rho_a = \frac{p}{RT} \tag{17}$$

where p = atmospheric pressure
ρ_a = air density
R = gas constant for dry air

T = absolute temperature

When vapor mass fraction of the air-vapor mixture, Y_v, is computed by the species balance equation, air density including effect of water vapor ρ is obtained by

$$\rho = \frac{M_{air}p}{RT\left((1-Y_v)+1.609Y_v\right)} \tag{18}$$

Specific humidity γ is computed in terms of partial pressures for water vapor and air.

$$\gamma = \frac{m_w}{m_a} = \frac{\rho_w}{\rho_a} = \left(\frac{M_w}{M_a}\right)\left(\frac{p_w}{p_a}\right) = 0.622\left(\frac{p_w}{p_a}\right) = 0.622\left(\frac{p_w}{p-p_w}\right) = 0.622\left(\frac{\phi p_{sat}}{p-\phi p_{sat}}\right) \tag{19}$$

p_w and p_a in Eq. (19) are partial pressures for water vapor and air, respectively. By using Dalton's law, specific humidity γ for a given relative humidity ϕ is computed in terms of saturation pressure p_{sat} as shown in the equation.

By using Eq. (19), the relationship between vapor mass fraction Y_v and relative humidity ϕ is obtained.

$$Y_v = \left(\frac{\gamma}{1+\gamma}\right) = \left(\frac{0.622\phi p_{sat}}{p-0.378\phi p_{sat}}\right) \tag{20}$$

The saturated pressure P_{sat} in Eq. (20) is expressed in Pa. The saturation pressure is calculated by Eq. (21) for a temperature T in K when water molecular weight M_{H2O} is 18 gm/mol.

$$p_{sat} = 611\exp\left[\left(\frac{M_{H2o}L}{R^*}\right)\left(\frac{1}{273.15}-\frac{1}{T}\right)\right] = 611\exp\left[9.0625L\left(\frac{1}{273.15}-\frac{1}{T}\right)\right] \tag{21}$$

where R^* is universal gas constant.

L in Eq. (21) is latent heat of vaporization in cal/gm.

$$L = 597.3 - 0.566(T-273.15), \text{ for absolute temperature T in K.} \tag{22}$$

Note that in the equation above, T will be the ambient dew point temperature if you want to compute the density of the air going into the cooling tower. If you want to compute the density of the air leaving the cooling tower, then T will be the temperature of the air after it has been warmed and moistened by contact with the hot water in the fill zone. Saturated pressure p_{sat} corresponding to droplet temperature, T_p, is computed by Eq. (21). Evaporation temperature, T_{vap}, is assumed to be saturated at the vapor pressure of the continuous air medium.

- Momentum Source Term F in the Momentum Conservation Equation

The present model calculates the superficial velocity based on volumetric flow rate. The porous media model incorporates an empirically determined flow resistance in a isotropic porous region. In essence, the isotropic porous media model is nothing more than an added momentum sink in the governing momentum equation Eq. (2). The source term is composed of two parts, a viscous loss term and an inertial loss term. It was based on Ergun's equation (1952).

$$F_i = -\left(\frac{\mu}{\alpha}v_i + \frac{1}{2}C\rho v_i^2\right)$$

(23)

where $\alpha = -\left(\frac{d_p^2 \varepsilon^3}{150(1-\varepsilon)^3}\right)$, and $C = -\left(\frac{3.5(1-\varepsilon)}{d_p \varepsilon^3}\right)$.

F_i in Eq. (23) is the momentum sink term in the direction i, where i = 1, 2, or 3, corresponding to the x-, y-, and z-direction, respectively. The coefficients α and C will be determined by pore porosity 77% and water droplet size of 3 mm.

- Energy Balance Equation in Porous Media

The present model calculates the energy transport equation given by Eq. (3) in porous zone with modifications to the transient terms and the conduction heat flux only. Total energy in the time derivative is used as the fluid-solid mixture energy, which is homogeneously mixed in terms of porosity. Thermal conductivity, $k_{h,eff}$, used in the conduction heat flux is used as the homogeneous mixture of fluid and solid conductivities.

$$k_{h,eff} = \varepsilon k_f + (1-\varepsilon)k_s$$

(24)

k_f and k_s in Eq. (24) are thermal conductivities for fluid and solid materials in porous media, respectively, assuming isotropic thermal contributions of solid material to the continuous fluid medium.

Boundary Conditions:

Boundary conditions for the modeling domain are provided for the following:
-   Wind speed and direction
-   Ambient temperature and humidity (vapor mass fraction)
-   Water inlet temperature
-   Fan speed
-   Water basin temperature for cooling tower system

The finite volume method with the adoption of an iterative procedure based on semi-implicit method for pressure-linked equations of pressure-velocity coupling is used in the present study. The gird distribution was non-uniform with smaller mesh size for the cell regions of the cooling tower as shown in Fig. 2. The present solution is not sensitive to the grid size when the number of total cells is higher than 2.5×10^6 for the H-Area tower as shown in Fig. 2. The iterative solution is considered as converged when the normalized residual errors of all the independent variables solved are reduced at least by three orders and the average exit air temperature is changed less than 0.01 $^{\circ}$C. The values of other variables have also been monitored during the iteration to make sure the convergent solution of all the variables at the end of iteration process.
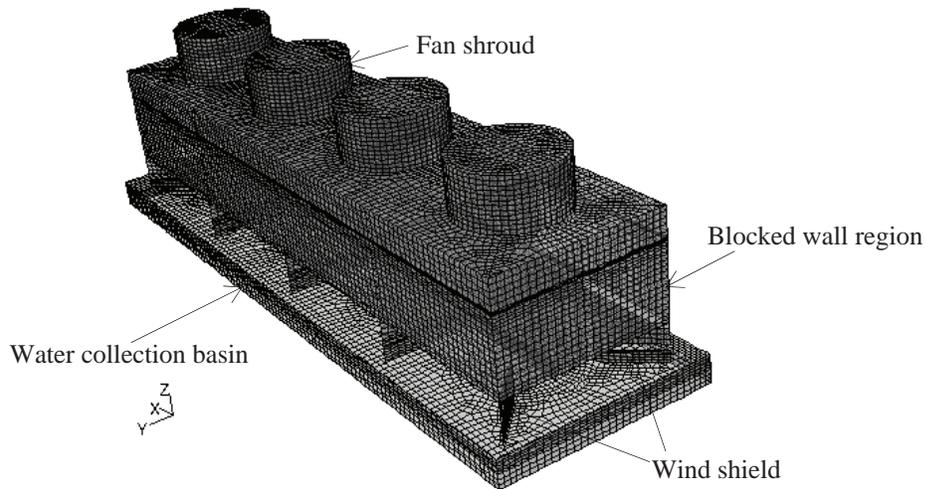
Figure 2. Computational meshes for the three-dimensional domains representing H-area countercurrent flow MDCT (2.5 x 10^6 meshes)

3. TEST DESCRIPTIONS AND MODEL VALIDATION

3.1 Experimental Measurement

Sensor locations for the measurements of key operating parameters and test results for the cross-flow MDCT are shown in the previous paper [2]. The compartment cells of the four-cell countercurrent-flow MDCT at SRS was instrumented at the exit of shroud region and near the water collection basin. Sensor locations for the measurements of key operating parameters are shown in Fig. 1. Air temperature and humidity measurements were made by using HOBO data logger [8] at six locations near the top of cooling fan shroud. Water temperatures at the cell exit were also measured by waterproof Tidbit data logger at 0.7m above the free surface of collection basin. Water flow rate and temperature at the inlet of the distribution deck were measured by Doppler ultrasonic meter and Tidbit, respectively. Measurement data for each sensor location were recorded at a time interval of 15 minutes during six-month period in 2005. Test data for ambient air temperature and humidity including wind speed and directions at the inlet of the cell were continuously obtained from SRNL meteorology station. The data recorded by the sensor logger were downloaded to the computer, and they were averaged over 1-hour period for the benchmarking database to validate the model. The measurement conditions and test results for each test case are summarized in Table I. The test results were used to benchmark and validate the integral model.

3.2 Model Validation

The analysis consists of two major parts. One part is to develop a model for the operation facility used to simulate countercurrent flow MDCT to benchmark the calculations with and without cooling fan operations. The second part is to calculate the flow patterns for the turbulent flow induced by fan and wind and to investigate fan and wind effects on water cooling inside the cell when cooling fans are operated and they are turned off.

The modeling work considers two basic cases with different operating conditions to examine how sensitive the flow patterns are to different fan and wind speeds. They are fast fan and no fan as shown in Table I. Flow patterns coupled with heat and mass transfer were calculated to evaluate the effect of water cooling inside the cell of the cooling tower. A three-dimensional CFD approach was used to solve the

governing equations for the flow domain as shown in Fig. 1. A prototypic geometry and domain of the cooling tower was created by a commercial finite volume code, FLUENT [9], and then it was meshed in non-orthogonal way to solve the governing equations. From the analysis of mesh sensitivity, about 2.5 million hexahedral meshes were established for the modeling calculations. The finite volume method with the adoption of an iterative procedure based on the semi-implicit method of pressure-velocity coupling was used for the study. The gird distribution was non-uniform with smaller mesh size for the cell regions of the cooling fan. The iterative solution is considered as converged when the normalized residual errors of all the independent variables solved are reduced at least by three orders and the average exit air temperature is changed less than 0.01°C. The values of other variables have also been monitored during the iteration to make sure the convergent solution of all the variables at the end of iteration process.

Drift eliminators inside the cells were modeled as porous media by using Ergun's equation [7]. About 77% porosity was estimated for the 0.15m thick drift region from the literature data as presented in the previous paper [2]. The flow conditions for the cooling tower operations are assumed to be fully turbulent since Reynolds numbers for typical operating conditions are in the range of 10^6. A standard two-equation turbulence model, referred to as $k-\varepsilon$ model [3], was used since benchmarking results against the literature data [10] showed that the model predicts turbulent flow evolution in a large fluid domain with reasonable accuracy [11]. Although other turbulent models such as RSM have the potential to give more accurate results for flows in which streamline curvature, swirl, rotation, or rapid changes near the wall boundary might be important, the standard $k-\varepsilon$ model is considered a good model for the current calculations over a large fluid domain of mechanical drift cooling tower with fully-developed turbulent flow medium. The results demonstrate that the $k-\varepsilon$ model combined with standard wall functions generally predicts the test results better than other models [11]. Its predictions agree with the data within about 15% [1,2].

The literature correlation [5,6] was used to calculate the heat and mass transfer from water droplets to the continuous gas phase at steady state, assuming them to be spherical and uniform. Based on the literature information [12] and computational efficiency, the model used the fixed droplet diameter to be 3 mm for the present analysis. The constitutive models for air pressure drops across the drift eliminator, turbulent flow characteristics, and water droplet heat transfer were benchmarked against the literature results [1]. The calculation results show that when single droplet is less than 4mm diameter, the model predicts the data by about 10% on the average. The experimental observations [13] clearly show that when droplet are larger than 4mm, it become non-spherical during free falling period. The integral benchmarking calculations for the counter-current MDCT used the uniform droplet size of 3 mm diameter based on the experimental observation performed by SRNL [1] and the literature information [12,13].

4. INTEGRAL BENCHMARKING RESULTS AND DISCUSSIONS

Modeling predictions for turbulent airflow behavior and heat transfer characteristics were benchmarked against the literature data conducted under the simple geometrical systems [2]. The verified model was extended to the prototypic countercurrent MDCT system coupled with air humidification process to perform the integral benchmarking tests. As shown in Table I, the test cases are typically two different air velocities at shroud exit, depending on the fan speeds of the cooling tower. They are normal fan speed with about 10 m/sec air speed and fan-off case with no forced convection. Average computational time for each of the test cases was about 4 days using two-cpu parallel run under HP DL585 Linux IBM workstation.

The modeling results show that when wind speed gets higher, air temperature inside the fan-off cell is distributed in more asymmetrical way across the upstream and downstream sides because heat transfer

performance from water droplet to air becomes better with air speed increased. These are consistent with the literature results [6]. From the modeling results, it is noted that when less humid air is introduced into the fan-off cell with high wind speed, it is humidified by the falling water with about the same level as that of the fan-on cell. Table II compares the results for vapor mass fractions at cell exit air for various ambient conditions under partially or totally fan-off cells. As shown in the table, it is noted that when less humid air is introduced into the fan-off cell with high wind speed, it is humidified by the falling water with about the same level as that of the fan-on cell.

The filed test data on the A-Area and H-Area MDCT's were used to benchmark the modeling simulation. Measurements were taken of the air inlet and exit temperatures, the ambient pressure, the water flow rate and its temperatures at the inlet and outlet. The detailed discussions of the measurement locations were provided in the previous section. Thirteen sets of the measured data from the A-Area tower and twenty sets of the H-Area test results are compared with the modeling predictions for the integral facilities. Key physical models for turbulence model, evaporative droplet cooling were validated against the literature data in the previous work [2]. The validated models were applied to the integral benchmarking test against the onsite test results for the A-Area and H-Area cooling towers. Comparison of the modeling predictions with the measured air exit temperatures for the A-Area and H-Area cooling towers is made in Fig. 3. The results show that the modeling predictions for the H-Area system are about 10% better than those of the A-Area system because of two potential reasons. One reason is that the model assumes uniform water distributions at the cell inlet, although the test results show that they are not uniform for the ambient and operating conditions. The other is probably due to the modeling assumption that an array of the staggered thin-rectangular plates for splitting the water droplets inside each cell has negligible impact on the cell residence time of the ambient air stream to be used for water cooling. Figure 3 also compares the modeling predictions with the measured vapor mass fractions at exit for A-Area and H-Area cooling towers. The model benchmarked here was applied to the evaluation of the wind impact on the air velocity at the exit of the cooling tower. The results show that when wind goes into the wide side of the A-Area tower with 90° and 270° angle directions relative to the plant north, only about 10 percent magnitude of the wind speed goes through the cooling cell region since each narrow side of the tower has a wall completely blocked to the wind.

The results show that when wind approaches toward the narrower side of the tower, cell exit velocity is at minimum due to the wind shield effect as shown in Fig. 1. It is also noted that as wind speed increases, air velocity at cell exit increases a little bit for the Bernoulli effect due to the presence of the flow obstructions. Quantitative results for the air exit speeds averaged over the shroud area show that the cell exit velocities from the H-Area countercurrent flow tower are less sensitive to the wind directions due to the difference of cooling cell design between the two towers, compared to those of the A-Area cross-flow tower.

Table I. Test conditions and results

Test cases (2005)	Ambient conditions			T_{wi} (^{o}C)	m_w kg/sec	$T_{cell, exit}$ (^{o}C), RH, (fan-on:1, fan-off:0)			
	T_{amb} (^{o}C)	RH	U_o, θ_o*			1st cell	2nd cell	3rd cell	4th cell
July21	24.40	0.86	0.71, 223	28.02	329.4	25.67, 0.99, (1)	25.56,1.0, (1)	25.23,1.0, (1)	28.02, 0.99, (1)
July22	25.17	0.80	0.81, 216	27.84	329.4	25.69, 0.98, (1)	25.56, 0.97, (1)	25.17, 0.96, (1)	25.17, 0.98, (1)
July26	28.22	0.68	1.0, 189	28.92	337.2	27.21, 0.98, (1)	26.73, 1.0, (1)	26.73, 1.0, (1)	26.73, 0.95, (1)
Aug8	27.44	0.77	1.25, 225	28.05	319.4	26.34, 0.97, (1)	26.34, 1.0, (1)	26.02, 1.0, (1)	26.03, 1.0, (1)
Aug14a	24.01	0.94	1.34, 169	26.15	316.1	24.40, 0.98, (1)	24.27, 0.97, (1)	24.08, 0.99, (1)	24.40, 0.99, (1)
Aug28	24.40	0.94	0.95, 56	27.56	449.2	25.95, 0.98, (1)	25.56, 0.99, (1)	25.46, 0.99, (1)	25.66, 1.0, (1)
Sep2	21.33	0.81	1.32, 344	22.72	416.8	21.71, 0.96, (1)	21.33, 0.95, (1)	21.14, 0.95, (1)	21.33, 0.95, (1)
Sep26a	21.33	0.98	2.04, 137	23.80	426.7	22.09, 1.0, (1)	22.09, 1.0, (1)	22.09, 1.0, (1)	22.09, 1.0, (1)
Sep28	27.12	0.70	4.06, 102	27.25	646.3	26.34, 0.97, (1)	25.76, 1.0, (1)	25.56, 1.0, (1)	25.95, 1.0, (1)
Sep29	19.60	0.97	0.63, 57	22.95	562.6	21.12, 1.0, (1)	21.16, 1.0, (1)	20.81, 1.0, (1)	21.02, 0.92, (1)
Sep29p	28.60	0.69	3.51, 278	25.46	635.1	25.13, 0.98, (1)	24.69, 1.0, (1)	24.98, 1.0, (1)	25.13, 0.97, (1)
Oct15	16.82	0.78	1.49, 179	18.22	369.3	16.95, 0.94, (0)	17.08, 0.95, (1)	16.63, 0.96, (1)	16.70, 0.95, (1)
Oct20	21.22	0.74	1.71, 188	22.62	380.7	21.49, 0.91, (0)	21.28, 0.91, (1)	21.11, 0.75, (0)	21.11, 0.87, (1)
Oct22	19.81	0.90	3.04, 274	24.19	391.3	22.09, 1.0, (0)	22.25, 1.0, (1)	22.25, 0.98, (0)	22.56, 1.0, (1)
Nov24	19.27	0.72	6.78, 268	24.65	477.1	23.24, 1.0, (0)	23.24, 1.0, (0)	23.24, 1.0, (0)	23.63, 1.0, (0)
Nov29	17.52	0.66	2.25, 231	20.62	511.6	19.33, 1.0, (1)	18.09, 1.0, (1)	20.19, 0.99, (0)	19.62, 1.0, (1)
Dec3	16.71	0.21	2.85, 160	22.07	442.1	22.31, 1.0, (0)	21.38, 1.0, (0)	21.60, 1.0, (0)	21.82, 1.0, (0)
Dec4	22.35	0.96	4.13, 197	24.04	549.0	23.57, 1.0, (0)	21.46, 1.0, (1)	22.80, 1.0, (0)	24.01, 1.0, (0)
Dec4m	20.19	1.0	2.43, 187	24.36	577.3	23.11, 1.0, (0)	21.58, 0.99, (1)	21.78, 0.97, (0)	21.46, 1.0, (0)
Dec5	17.67	1.0	2.80, 188	23.17	676.8	20.57, 1.0, (0)	19.89, 1.0, (1)	20.34, 1.0, (1)	18.96, 1.0, (0)

Note: *U_o θ_o are wind speed and direction with respect to true North, respectively
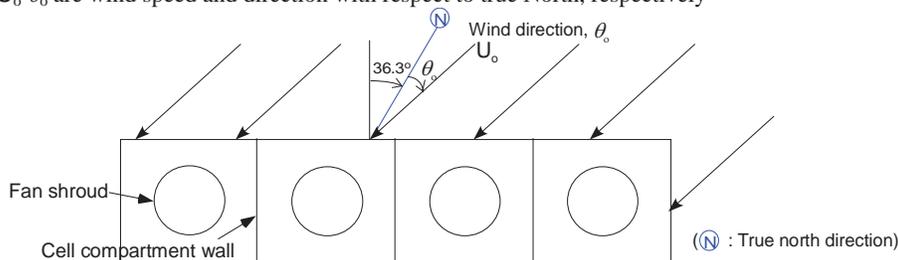
Table II. Results for vapor mass fractions at cell exit for various ambient conditions under partially or totally fan-off cases

Cases	Ambient conditions			Averaged vapor mass fraction at cell exit (γ_{exit})			
	T_{amb}	γ_{amb}	U_o	Fan-off cell		Fan-on cell	
				Data	Pred.	Data	Pred.
Oct15	16.82	0.0092	1.49	0.0112	0.0102	0.0113	0.0112
Oct20	21.22	0.0115	1.71	0.0144	0.0136	0.0131	0.0130
Oct22	19.81	0.0129	3.04	0.0165	0.0178	0.0168	0.0167
Nov24	19.27	0.0100	6.78	0.0181	0.0180	--	--
Dec3	16.71	0.0025	2.85	0.0162	0.0151	--	--
Dec4	22.35	0.0161	4.13	0.0179	0.0177	0.0159	0.0177
Dec4m	20.19	0.0147	2.43	0.0164	0.0160	0.0158	0.0177
Dec5	17.67	0.0125	2.80	0.0143	0.0146	0.0146	0.0155
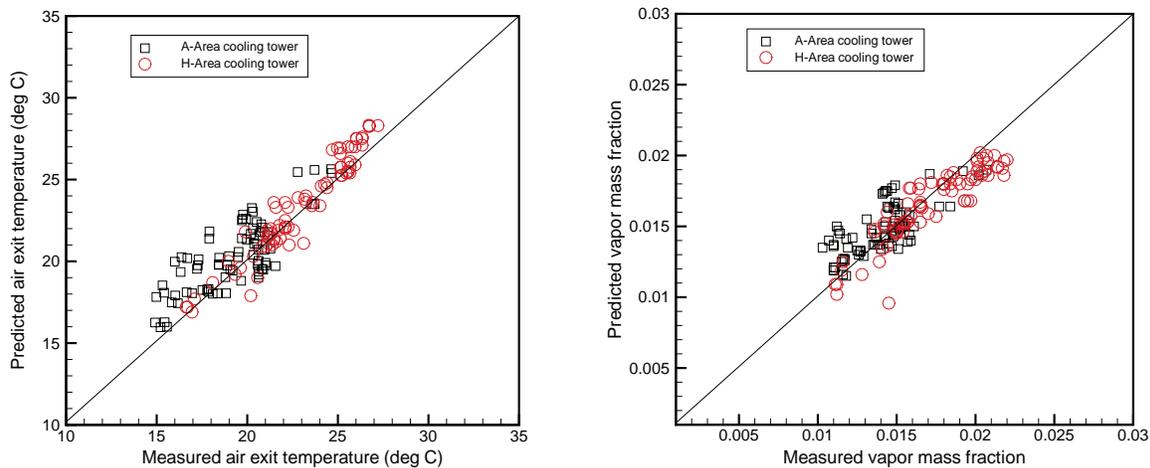
Figure 3. Comparison of the modeling predictions with the measured air exit results for A-Area (cross-flow) and H-Area (countercurrent flow) cooling towers

5. CONCLUSION

A three-dimensional steady-state CFD model was developed for the SRS four-cell MDCT system to evaluate the flow patterns and heat transfer characteristics inside the cooling cell driven by cooling fan and wind. It used standard two-equation turbulence model to capture turbulent flow behavior of air inside and outside the tower cells. The model considers the air-vapor mixture coupled with water droplet component, assuming that vapor phase is always transported by the continuous air phase with no slip velocity. In this work, water droplet component was considered as discrete phase via Lagrangian approach for the evaporative heat transfer. Experiments were conducted to obtain the benchmarking database for verifying the CFD model.

A series of the modeling calculations was performed to investigate the impact of the ambient and operating conditions on flow patterns and heat transfer characteristics inside the cell of the counter-current cooling tower. The modeling predictions are in reasonably good agreement with the test results. It is also demonstrated that CFD method is applicable to the detailed modeling analysis for the large-scaled cooling tower system.

REFERENCES

1. S. Y. Lee, A. J. Garrett, and J. S. Bollinger, "CFD Modeling and Analysis for A-Area and H-Area Cooling Towers", SRNL-STI-2009-00137, Savannah River National Laboratory, August (2009).
2. S. Y. Lee, A. J. Garrett, J. S. Bollinger, and L. D. Koffman, " CFD Modeling Analysis of Mechanical Draft Cooling Tower ", *Proceedings of ASME 2008 Summer Heat Transfer Conference*, Paper No. HT2008-56080, Jacksonville, Florida, August 10-14 (2008).
3. W. P. Jones and P. E. Launder, "The Prediction of Laminarization with a Two-Equation Model of Turbulence", *Int. J. of Heat and Mass Transfer*, **15**, pp. 301-314 (1972).
4. S. A. Morsi and A. J. Alexander, "An Investigation of Particle Trajectories in Two-Phase Flow Systems", *J. of Fluid Mechanics*, **55**, pp. 193-208 (1972).
5. D. P. Kessler and R. A. Greenkorn, *Momentum, Heat Mass Transfer Fundamentals*, Mercel Dekker, Inc., New York (1999).
6. W. E. Ranz and W. R. Marshall, Jr., "Part II, Evaporation from Drops", *Chemical Eng. Progress*, **48**, pp. 173-180 (1952).
7. S. Ergun, "Fluid through Packed Columns", *Chemical Eng. Progress*, **18**(2), pp. 87-94 (1952).
8. HOBO Water Temp Pro Logger, www.microdaq.com.
9. FLUENT, ANSYS, Inc., Lebanon, New Hampshire (2012).
10. P. V. Nielsen, A. Restivo, and J. H. Whitelaw, "The Velocity Characteristics of Ventilated Rooms", ASME *J. of Fluids Engineering*, **100**, pp. 291-298 (1978).
11. S. Y. Lee, R. A. Dimenna, R. A. Leishear, D. B. Stefanko, "Analysis of Turbulent Mixing Jets in a Large Scale Tank", ASME *J. of Fluids Engineering*, **130** (1), pp. 011104 (2008).
12. S. P. Fisenko, A. A. Brin, and A. I. Petruchik, "Evaporative Cooling of Water in a Mechanical Draft Cooling Tower", *Int. J. of Heat and Mass Transfer*, **47**, pp. 165-177 (2004).
13. S. C. Yao and V. E. Schrock, "Heat and Mass transfer from Freely Falling Drops", Trans. ASME *J. of Heat Transfer*, **98**, pp. 120-126 (1976).